Article

Structural, Optical, and Electrical Properties of Copper Oxide Films Grown by the SILAR Method with Post-Annealing

Wen-Jen Lee * and Xin-Jin Wang

Department of Applied Physics, National Pingtung University, Pingtung 900, Taiwan; jim40929@gmail.com
* Correspondence: wenjenlee@mail.nptu.edu.tw

Abstract: Copper oxides are widely used in photocatalysts, sensors, batteries, optoelectronic, and electronic devices. In order to obtain different material properties to meet the requirements of different application fields, varied technologies and process conditions are used to prepare copper oxides. In this work, copper oxide films were grown on glass substrates by a successive ionic layer adsorption and reaction (SILAR) method with subsequent annealing under an atmospheric environment. The films were characterized by using an X-ray diffractometer, Raman spectrometer, Scanning electron microscope, UV-Visible-NIR spectrophotometer, and Hall Effect measurement. The results show that the as-deposited film has a Cu_2O crystal structure, which begins to transform into Cu_2O-CuO mixed crystal and CuO crystal structure after annealing at 300 °C for a period of time, resulting in the bandgap of being reduced from 1.90 to 1.34 eV. The results show that not only are the crystal structure and bandgap of the films affected by the post-annealing temperature and time, but also the resistivity, carrier concentration, and mobility of the films are varied with the annealing conditions. In addition, the film with a Cu_2O-CuO mixed crystal shows a high carrier mobility of 93.7 $cm^2 \cdot V^{-1} \cdot s^{-1}$ and a low carrier concentration of 1.8×10^{12} cm^{-3} due to the formation of a Cu_2O-CuO heterojuction.

Keywords: copper oxide; Cu_2O; CuO; successive ionic layer adsorption and reaction; SILAR

1. Introduction

Copper oxide has two typical crystalline forms as cupric oxide (tenorite monoclinic CuO) and cuprous oxide (cuprite cubic Cu_2O) that the CuO and Cu_2O are well-known p-type semiconductors with a bandgap energy of about 1.3–2.1 and 2.1–2.6 eV, respectively [1]. In addition, CuO and Cu_2O have been widely studied in similar applications such as photocatalysts [2,3], gas sensors [4,5], photodetectors [6,7], solar cells [8,9], batteries [10,11], supercapacitors [12,13], and so forth. A variety of techniques including sputtering [9,14], evaporation [15,16], thermal oxidation [17,18], sol-gel [19,20], spray pyrolysis [21,22], electrodeposition [23,24], and successive ionic layer adsorption and reaction (SILAR) method [25–30] have been employed to synthesize copper oxide films.

The SILAR method is a modified chemical bath deposition (CBD) developed by Nicolau in 1985 [31]. It has the characteristics of being low cost, having a low process-temperature, precise film-thickness control, and being suitable for large-area deposition. This is different from the typical CBD process, where all chemicals are present in the reaction vessel at the same time for film deposition. In the SILAR process, the cation and anion precursor solutions are stored in separate containers, and the substrate is sequentially immersed in the cation and anion precursor solutions, and the substrate is rinsed with high-purity deionized water (DI-water) after each immersion. Generally, a reaction cycle of SILAR process includes four steps. In the first step, the substrate is immersed in the cation precursor solution, and the cations will be chemically adsorbed on the negatively charged surface of the substrate. In the second step, the substrate is rinsed with DI-water to remove the extra amount reactants, leaving only a saturated chemisorption layer of cations. In

the third step, the substrate is immersed in the anion precursor solution, and the anions will react with the chemically adsorbed cations to form a thin film of solid compound on the surface of the substrate. In the fourth step, rinse the substrate again with deionized water to remove excess reactants, and leave a surface to start a new cycle. From step 1 to step 4, a SILAR reaction cycle is completed, and the thickness of the deposited film can be increased and controlled by controlling the number of reaction cycles. Since the film growth mechanism of SILAR is the layer-by-layer stacking of ions, SILAR is also called solution atomic layer deposition (SALD) [32] or liquid atomic layer deposition (LALD) [33].

So far, several different cation and anion precursor solutions have been used in the SILAR process to grow copper oxide films. For example, Bayansal et al. [34] used a copper chloride solution and double distilled water to synthesize dense and continuous CuO films with plate-like nanostructures, and the bandgap energies of as-deposited and annealed films at 300 °C for 1 h are about 1.37 and 1.39 eV, respectively. Magshwari et al. [26] used a tetraamine copper complex solution and deionized water as cation and anion precursors to deposit nanocrystalline and single-phase CuO films on glass substrates by SILAR, and showed that the film-thickness of CuO was proportionally increased from 87 to 415 nm with increasing the SILAR reaction-cycles from 20 to 50 times. Jayakrishana et al. [35] used copper acetate and sodium acetate as cation and anion precursors to grow CuO films on glass substrates by SILAR, and then the CuO films were annealed at temperatures of 100–400 °C in a vacuum environment. The results showed that the bandgap energy of CuO films is increased from 1.31 to 2.06 eV by vacuum-annealing, resulting in preferential crystal growth along the (200) plane.

In 1985, Ristov et al. [36] reported for the first time a simple chemical deposition method for depositing Cu_2O films on glass substrates that the method includes successively immersing the glass substrates in a copper thiosulfate complex and a NaOH solution for 1–2 s each, and the film-thickness is proportional to the number of reaction-cycles for the successive immersion, and it is noticed that this method is very similar to the SILAR method proposed by Nicolau in the same year (1985) [31]. After that, many research groups extensively use the same precursors to grow Cu_2O films in the SILAR process. For example, Nair et al. [37] used the same copper thiosulfate complex and NaOH precursor solution to prepare Cu_2O films on glass substrates, and found that, after the films were annealed in air at 350 °C, the crystal structure of the films changed from Cu_2O to CuO, resulting in the optical bandgap of the films being reduced from 2.1 to 1.75 eV. Serin et al. [38] used the same cation and anion precursor to deposit about 0.15 μm-thick Cu_2O films on glass substrates, and then the films were annealed from 200 to 350 °C for 1 h in air. The results showed that the as-deposited film and the films annealed at 200–250 °C are Cu_2O, but the films are converted to CuO when annealed above 300 °C. In addition, this conversion is accompanied by a shift in the optical bandgap from 2.20 to 1.35 eV. Johan et al. [39] prepared Cu_2O films on glass substrates with thickness of about 0.45 μm by using similar reaction precursors and annealed the films at 200–400 °C in air. They found that the as-deposited and 200 °C-annealed films are Cu_2O, and the films annealed at 300 °C have both Cu_2O and CuO coexisting phases, and the films annealed at 400 °C have single-phase CuO. In addition, the optical bandgap of the films is decreased from 2.40 to 1.73 eV because the crystalline phase of the films is changed from Cu_2O to CuO by annealing.

These reports indicate that the as-deposited film synthesized from the precursor solutions of copper thiosulfate complex and NaOH by the SILAR method usually has single-phase Cu_2O, which can be transferred to the CuO film by further annealing in air at a temperature above 300 °C. Nevertheless, Ravichandran et al. [40] reported that as-growth films synthesized from the reaction precursors of a copper thiosulfate complex solution and a NaOH solution have single-phase CuO, even if the immersion time varies from 15 to 30 s.

So far, the morphology, structure, and optical properties of copper oxide films prepared by the SILAR method under various synthesis conditions have been studied. However, as far as we know, there are few studies on the influence of thermal annealing on the electrical
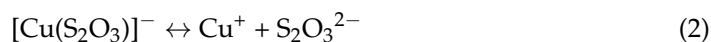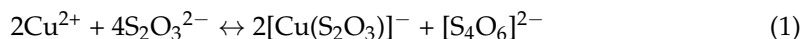
properties (resistivity, carrier concentration, and mobility) of the SILAR-grown Cu_2O thin films phase-transforming into CuO thin film analyzed by Hall measurement.

Therefore, in this work, copper thiosulfate complex and NaOH solutions are used as cation and anion precursor solutions to grow Cu_2O thin films on glass substrates by the SILAR method. In addition, in order to obtain films of different crystal-phases (Cu_2O, Cu_2O-CuO mixture, and CuO), the as-growth Cu_2O films are subsequently annealed in air at temperatures of 200–300 °C for 1 to 4 h. Furthermore, not only the morphological, structural, and optical properties of the films are characterized but also the electrical properties (resistivity, carrier concentration, and mobility) are analyzed. In addition, the influence of thermal annealing on the relationship among morphological, structural, optical, and electrical properties are discussed.

2. Materials and Methods

2.1. Samples Preparation

In this work, general glass slides were used as substrates for the growth of Cu_2O films by the successive ionic layer adsorption and reaction (SILAR) method. The substrates were cleaned in an ultrasonic bath sequentially using deionized water, acetone, and methanol for 10 min each, followed by drying in a nitrogen flow. A copper thiosulfate complex and a NaOH solution were used as a cation and anion precursor solution in the SILAR process, respectively. To prepare the cation precursor solution, 1 M cupric sulfate pentahydrate ($CuSO_4 \cdot 5H_2O$) was added into 1 M sodium thiosulfate ($Na_2S_2O_3 \cdot 5H_2O$), and then the mixed solution was magnetically stirred for 20 min to immediately obtain a colorless solution of copper thiosulfate (CuS_2O_3) complex (the chemical reaction as shown in Equation (1)). Preparing the anion precursor solution, 1 M NaOH solution was heated and kept at 70 °C. Depositing Cu_2O thin films on glass substrates by the SILAR method included four steps; in the first step, the glass substrate was first immersed in the NaOH solution for 20 s, and the OH^- ions will be chemically adsorbed to the surface of the substrate in this step. In the second step, the substrate was then taken out and rinsed with deionized water to remove excessive OH^- ions, which were not adsorbed on the surface of the substrate. In the third step, the substrate was immersed in the solution of copper thiosulfate (CuS_2O_3) complex for 20 s; in this step, the dissociative Cu^+ ions [as Equation (2)] will react with OH^- ions (adsorbed on the substrate surface) to form a Cu_2O thin film [as Equation (3)] on the surface of the substrate. In the fourth step, the substrate was taken out and rinsed with deionized water again to remove the reaction byproduct and unreacted precursor solution. From steps 1 to 4, one SILAR reaction-cycle is completed, and the thickness of the films can be increased and controlled by increasing the number of reaction-cycles. In this work, the films were obtained through 80 SILAR reaction-cycles, and the thickness of the films was about 500 nm. After the films were deposited, the as-growth Cu_2O films were subsequently annealed in air at temperatures of 200–300 °C for 1 to 4 h:

$$2Cu^{2+} + 4S_2O_3^{2-} \leftrightarrow 2[Cu(S_2O_3)]^- + [S_4O_6]^{2-} \tag{1}$$

$$[Cu(S_2O_3)]^- \leftrightarrow Cu^+ + S_2O_3^{2-} \tag{2}$$

$$2Cu^+ + 2OH^- \rightarrow Cu_2O + H_2O \tag{3}$$

2.2. Samples Characterization

The crystalline structures of the copper oxide thin films were examined by an X-ray diffractometer (XRD, D8 Advance Eco, Bruker, Karlsruhe, Germany) using a grazing incidence XRD mode at an X-ray wavelength of 0.15418 nm, a voltage of 40 kV, and a current of 25 mA. The Raman spectra of the films were performed by a micro Raman spectrometer (Raman, UniRAM II, Uninanotech, Yongin, Korea) using a green laser with a wavelength of 532 nm and an optical power of 300 mW. The surface morphologies of the films were observed with a high-resolution field-emission scanning electron microscope (FESEM, SU8000, Hitachi, Tokyo, Japan). It is noted that, in order to obtain the true

surface morphologies of the films, both the SEM surface and cross-sectional analysis were performed without any conductive coating on the films. Moreover, the samples used for cross-sectional SEM analysis must have an undamaged fracture surface for which the preparation method of samples is detailed in Part 1 of Supplementary Materials (Figure S1). The optical properties of the films were analyzed by a UV-Visible-NIR spectrophotometer with a 60 mm diameter integral sphere (UV-Vis-NIR, V-670, Jasco, Tokyo, Japan). The electrical properties (resistivity, carrier concentration and mobility) of the films were measured by a Hall Effect measurement system (Hall, VDP6800, Sadhudesign, Hsinchu, Taiwan) using the Van der Pauw method under a 5600 Gauss magnetic field at room temperature. In addition, the preparation method of samples for Hall Effect measurement is described in detail in Part 2 of the Supplementary Materials (Figure S2).

3. Results and Discussion

In order to identify the crystalline structure of the copper oxide films, the films were analyzed by X-ray diffraction (XRD). Figure 1 shows the XRD patterns of as-deposited and annealed copper oxide films grown on glass substrates by the SILAR method. According to the XRD patterns, the as-deposited and 200 °C-annealed films have a polycrystalline structure with single-phase Cu_2O, and the films annealed at 300 °C for 2 and 3 h have a polycrystalline structure with single-phase CuO. In particular, the film annealed at 300 °C for 1 h has a two-phase mixed polycrystalline structure containing Cu_2O and CuO phases. Obviously, 300 °C is the phase-transition temperature at which the Cu_2O film is transformed into a CuO film by thermal annealing in the air. In addition, from XRD pattern of the Cu_2O-CuO mixed film (as Figure 1c), it can be clearly observed that the intensities of the Cu_2O XRD-peaks are very weak (almost disappearing), indicating that the film is mainly composed of CuO and contains a small amount of Cu_2O.
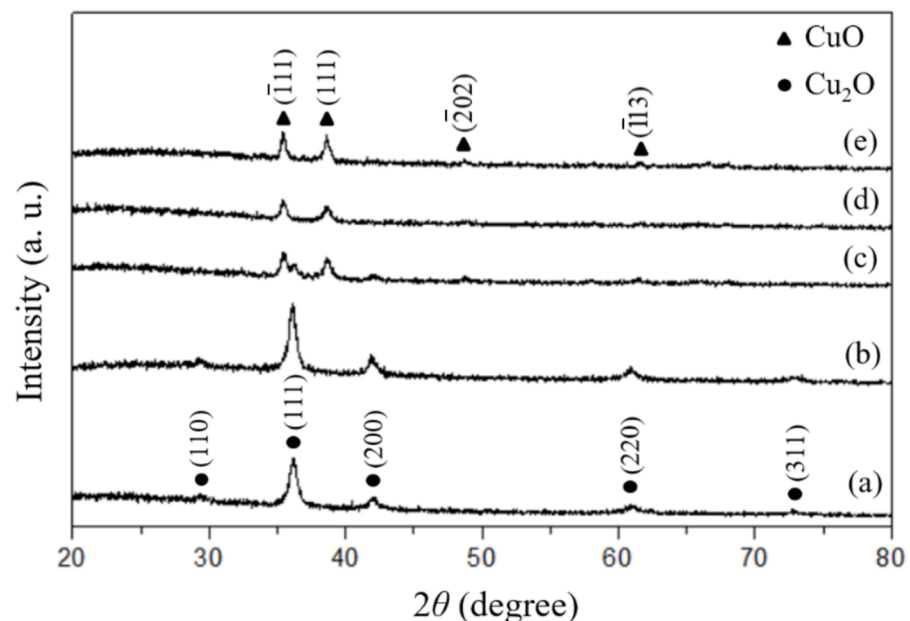

Figure 1. XRD patterns of copper oxide films: (**a**) the as-deposited film; (**b**) the film annealed at 200 °C for 1 h, and the films annealed at 300 °C for (**c**) 1; (**d**) 2; and (**e**) 4 h, respectively.

In Figure 1a, the as-deposited film has a polycrystalline structure with single-phase Cu_2O that has five clear XRD peaks located at 2θ of 29.5°, 36.4°, 42.2°, 61.3°, and 73.5° that can be corresponded to (110), (111), (200), (220), and (311) planes of cuprite Cu_2O (JCPDS No.: 05-0667), respectively. In addition, both as-deposited and 200 °C-1 h annealed Cu_2O films have a (111) preferred orientation of crystal growth that is confirmed by the texture

coefficients of the Cu_2O films as shown in Table 1. The texture coefficient (TC) is calculated by using the Harris method [41] as below:

$$TC_{hkl} = \frac{I_{hkl} / I_{hkl}^o}{(1/n) \sum (I_{hkl} / I_{hkl}^o)} \tag{4}$$

where I_{hkl} is the measured intensity of XRD peak, I_{hkl}^o is the standard intensity of Cu_2O powder obtained from the JCPDS database, and n is the number of the XRD peaks. Moreover, the (111) peak-intensity of 200 °C-1 h annealed Cu_2O film is stronger than the as-deposited Cu_2O film and the full width at half maximum (FWHM) of the (111) peak of 200 °C-1 h annealed Cu_2O film is smaller than the as-deposited Cu_2O film, indicating that the crystallinity of Cu_2O film is apparently improved by thermal annealing (as Figure 1a,b). Similar crystallinity improvement is also occurred in the CuO films annealed at 300 °C by increasing the annealing time. In addition, the phenomenon of grain growth and coarsening is also observed from the high-resolution SEM images, which will be explained later.

Table 1. Texture coefficients for the different crystal orientations of the as-growth and 200 °C-1 h annealed Cu_2O films.

Samples	Texture Coefficient (TC)				
	(110)	**(111)**	**(200)**	**(220)**	**(311)**
(a) as-deposited	0.873	1.429	1.028	0.907	0.761
(b) 200 °C-1 h annealed	0.854	1.495	1.041	0.954	0.654

In addition to XRD, Raman spectroscopy is also a technique commonly used to identify the crystalline structure of materials. Figure 2 shows the Raman spectra of as-deposited and annealed copper oxide films grown on glass substrates by SILAR. Two distinct Raman patterns can be clearly seen in Figure 2, one of which is Figure 2a,b, and the other similar group is Figure 2c–e. The two different Raman patterns are attributed to the two different crystal structures of Cu_2O and CuO. For Figure 2a,b, six Raman peaks are observed at about 109, 140, 212, 276, 310, and 610 cm^{-1} that show the characteristic phonon frequencies of the crystalline Cu_2O. According to the literature [42–47], the peak at 109 cm^{-1} is assigned to the inactive Raman mode, the peak at 140 cm^{-1} is ascribed to Raman scattering from phonons of symmetry Γ^-_{15}, the peak at 212 cm^{-1} is from the second-order Raman-allowed mode, the peak at 310 cm^{-1} corresponds to the second-order overtone mode, and the peak at 610 cm^{-1} is attributed to the infrared-allowed mode. However, the corresponding Raman mode of the peak at 276 cm^{-1} is not found in the literature. For the Figure 2c–e, four Raman peaks located at about 120, 281, 329, and 614 cm^{-1} are detected that show the characteristic phonon frequencies of the crystalline CuO. According to the literature [48–50], the peaks at 281, 329, and 614 cm^{-1} are from one-phonon Raman scattering mode of CuO crystal, where 281 cm^{-1} belongs to the A_g mode, 329 and 614 cm^{-1} belong to the B_g mode. The peak at 120 cm^{-1} is unknown, but it was also found from earlier reports [50]. In addition, although the XRD pattern (Figure 1c) shows that the film has a mixed crystal structure with CuO as the main component and a small amount of Cu_2O after annealing at 300 °C for 1 h, only the Raman peaks of CuO can be observed in the Raman spectrum (Figure 2c) without Cu_2O. This is because some Raman peaks of Cu_2O crystal are very close to Raman peaks of CuO, and the content of Cu_2O in the film is relatively small, resulting in the Raman signal of Cu_2O not being detected.
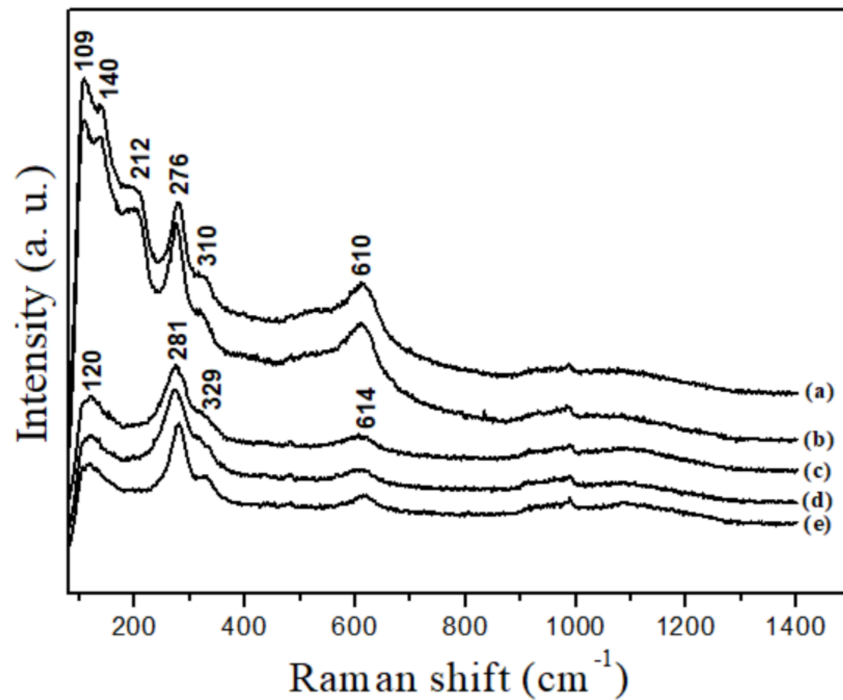
Figure 2. Raman spectra of copper oxide films: (**a**) the as-deposited film; (**b**) the film annealed at 200 °C for 1 h, and the films annealed at 300 °C for (**c**) 1; (**d**) 2; and (**e**) 4 h, respectively.

The surface morphologies of copper oxide films grown by SILAR are shown in Figure 3. As shown in Figure 3a, irregular microsphere particles can be observed to accumulate on the surface of the deposited film. The presence of these particles can be regarded as an inevitable phenomenon in the solution-based process. In addition, the inset image in Figure 3a shows that the profile of the as-deposited film (thickness about 500 nm) is dense and uniform. It can be seen from Figure 3b that, when the film is annealed at 200 °C for 1 h, some larger particles will be formed on the film. However, it can be found from Figure 3c that annealing the film at 300 °C for 1 h does not seem to change the size of these particles, which is mainly due to the mixed Cu_2O-CuO phase of the film at this stage. When the annealing time was increased to 2 h, these particles aggregated into irregular clusters on the film. In addition, as the annealing time is extended to 4 h, it can be noted that the agglomeration of these clusters leads to the formation of larger stacks on the film. On the other hand, it can be observed from the high-resolution SEM images that the particles on the surface of the as-growth film are approximately spherical in shape and have a smooth surface. After annealing at 200 °C for 1 h, many spherical and isolated small crystal grains (grain size of about 43–74 nm) are uniformly distributed and appeared on the smooth surface of the particles. When the annealing temperature is increased to 300 °C, it can be clearly observed that the particles on the surface of the films are composed of many irregularly shaped grains, thus forming a rough surface. Moreover, the grain size increases with the increase of thermal annealing time such that the grain size can reach about 141–192 nm after annealing at 300 °C for 4 h. This can be explained by diffusion-controlled coarsening kinetics (i.e., Ostwald ripening). Since the diffusion of the materials is proportional to temperature and time, the diffusion rate of atoms is low at a temperature of 200 °C without significant Ostwald ripening. Therefore, isolated spherical crystal grains appear on the surface of the 200 °C-1 h annealed film. However, atoms have a higher diffusion rate at a temperature of 300 °C, the phenomenon of grain coalescence leads to irregular grain shapes, and the grain size increases with the increase of annealing time.
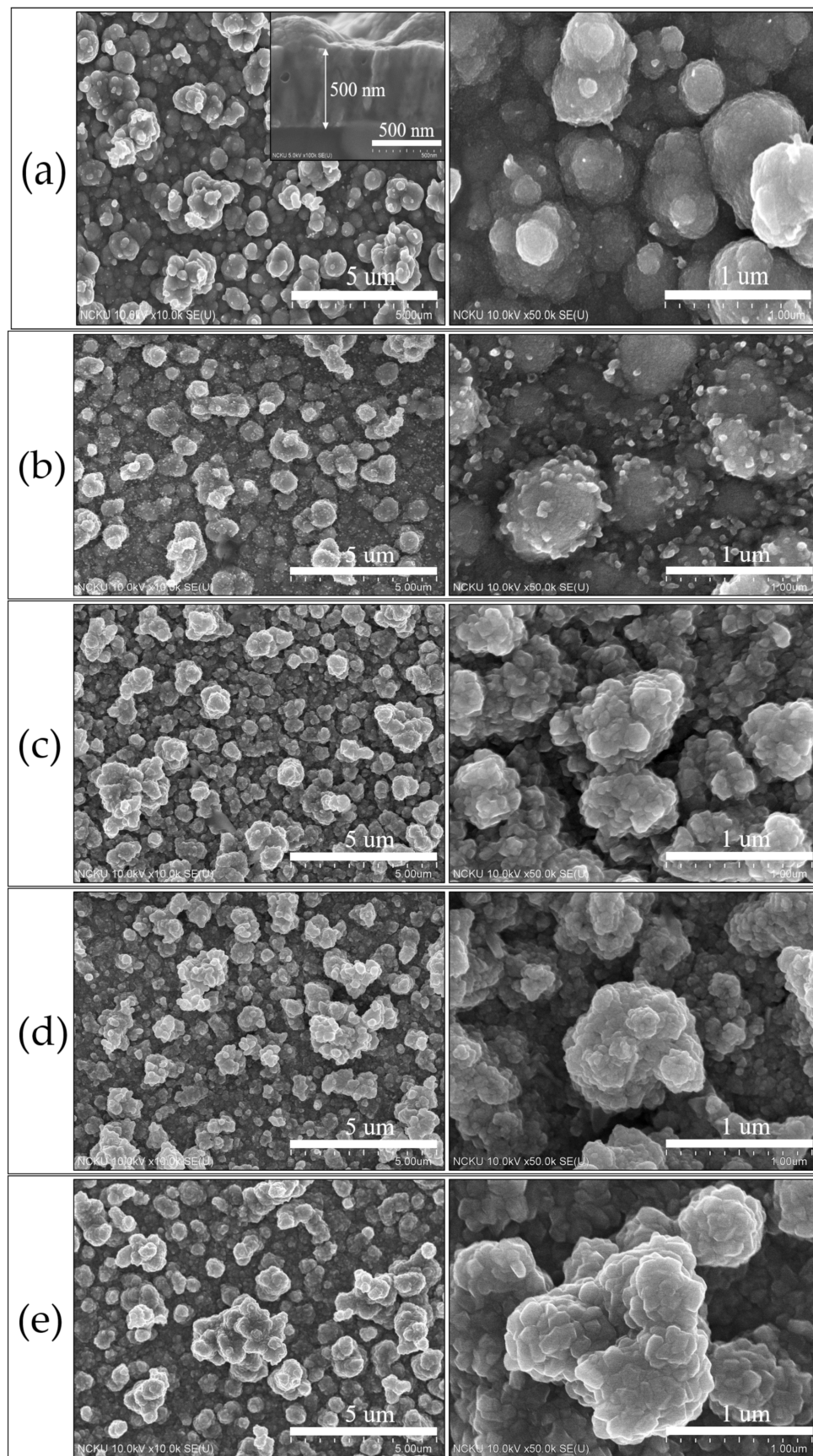
Figure 3. The surface morphologies of copper oxide films: (**a**) the as-deposited film (the insert shows its cross-section); (**b**) the film annealed at 200 °C for 1 h, and the films annealed at 300 °C for (**c**) 1; (**d**) 2; and (**e**) 4 h, respectively.

In order to evaluate the optical bandgaps of the copper oxide films, the transmittance (T) and reflectance (R) spectra of the films were measured using a UV-Vis-NIR spectrophotometer with a 60 mm diameter integral sphere (Jasco V-670), and the absorbance (A) was derived from the calculation of A = 100 − (T + R) (%) to obtain the absorption spectra (Figure 4) of the films [51], and then the bandgap energies of the films were extracted from the plots of $(Ahv)^2$ vs hv (as shown in Figure 5). As shown in Figure 5, the bandgaps are about 1.90, 1.87, 1.40, 1.36, and 1.34 eV for as-deposited (Figure 5a), 200 °C-1 h annealed (Figure 5b), 300 °C-1 h annealed (Figure 5c), 300 °C-2 h annealed (Figure 5d), and 300 °C-4 h annealed (Figure 5e) films, respectively. The results show that, because 300 °C thermal annealing causes the films to transform from Cu_2O to CuO crystal phase, thus the bandgap energies of the films are greatly reduced from 1.87–1.90 to 1.34–1.40 eV. In addition, although the film after annealing at 300 °C for 1 h has a two-phase mixed crystal structure of containing both CuO and Cu_2O, the bandgap energy of film only shows the CuO feature (~1.40 eV) due to a few contents of Cu_2O in the film. Moreover, it is known from the experimental results that the energy gap of the copper oxide film can be adjusted by thermal annealing. It can be reasonably imagined that, if the annealing conditions are accurately controlled to adjust the ratio of Cu_2O and CuO crystalline phases, there will be an opportunity to accurately control the bandgap of the copper oxide film within the range of 1.90 to 1.34 eV.
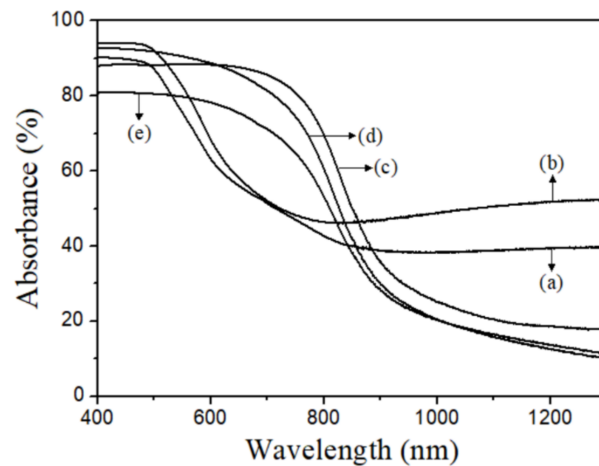

Figure 4. The absorption spectra of copper oxide films: (**a**) the as-deposited film; (**b**) the film annealed at 200 °C for 1 h; and the films annealed at 300 °C for (**c**) 1; (**d**) 2; and (**e**) 4 h, respectively.
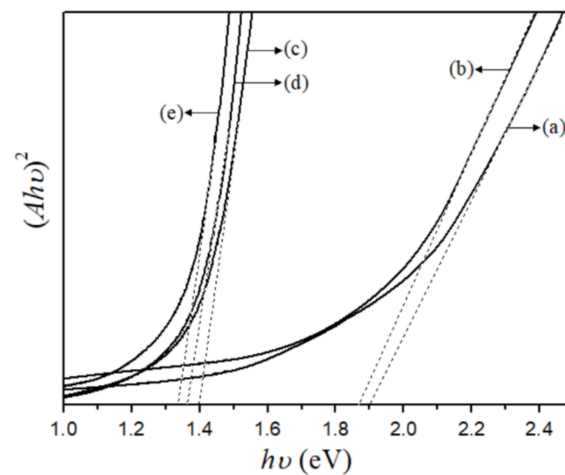

Figure 5. The bandgap energies of copper oxide films extracted from the plots of $(Ahv)^2$ vs. hv: (**a**) the as-deposited film; (**b**) the film annealed at 200 °C for 1 h; and the films annealed at 300 °C for (**c**) 1; (**d**) 2; and (**e**) 4 h, respectively.

The resistivity, carrier concentration, and mobility of the copper oxide films measured by Hall Effect measurement are shown in Figure 6, and a summary of crystalline structure, bandgap energy, resistivity, carrier concentration, and mobility of the copper oxide films are listed in Table 2.
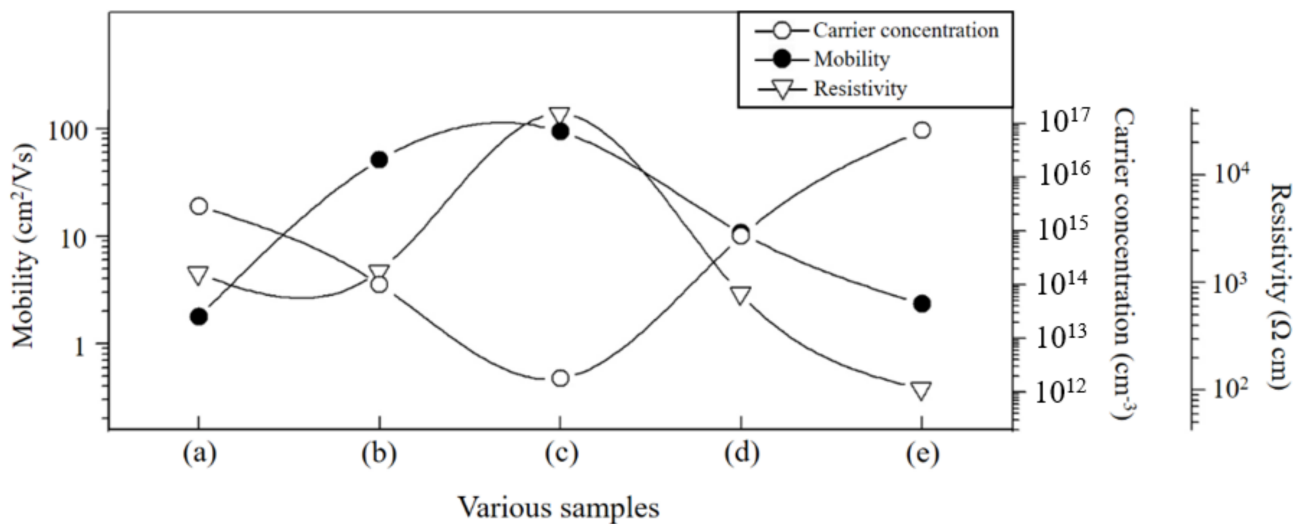

Figure 6. Resistivity, carrier concentration, and mobility of the copper oxide films: (**a**) the as-deposited film; (**b**) the film annealed at 200 °C for 1 h, and the films annealed at 300 °C for (**c**) 1; (**d**) 2; and (**e**) 4 h, respectively.

Table 2. Summary of crystalline structure, bandgap energy, resistivity, carrier concentration, and mobility of the copper oxide films.

Samples	Crystal Structure	Bandgap Energy (eV)	Resistivity (Ω-cm)	Carrier	
				Concentration (cm^{-3})	Mobility (cm^2·V^{-1}·S^{-1})
(a) as-deposited	(Cu$_2$O)	1.90	1.22×10^3	2.9×10^{15}	1.8
(b) 200 °C-1 h annealed	(Cu$_2$O)	1.87	1.27×10^3	1.0×10^{14}	51.1
(c) 300 °C-1 h annealed	(CuO-Cu$_2$O mixture)	1.40	3.72×10^4	1.8×10^{12}	93.7
(d) 300 °C-2 h annealed	(CuO)	1.36	7.94×10^2	8.0×10^{14}	10.7
(e) 300 °C-4 h annealed	(CuO)	1.34	1.02×10^2	7.4×10^{16}	2.3

The results show that, just as the crystal structure and bandgap of the copper oxide films change with the annealing temperature and time, the resistivity, carrier concentration, and mobility of the copper oxide films also change with the annealing temperature and time.

After 200 °C-1 h thermal annealing, the carrier mobility of the film increased from 1.8 to 51.1 cm^2·V^{-1}·s^{-1}, and the carrier concentration of the film decreased from 2.87×10^{15} to 1.0×10^{14} cm^{-3}, which can be attributed to the improvement of crystal quality and the reduction of crystal defects, and the increase in carrier mobility and decrease in carrier concentration result in almost the same resistivity of the 200 °C-1 h annealed film to the as-deposited film.

However, the carrier concentration of the film annealed at 300 °C for 1 h subsequently dropped by about two orders of magnitude, reaching 1.8×10^{12} cm^{-3}, which is the lowest value compared with the carrier concentration of other films. Since the 300 °C-1 h annealed

film has a Cu_2O-CuO mixed crystal, the sudden decrease in the carrier concentration of the film can be reasonably attributed to the formation of Cu_2O-CuO heterojunction, which results in recombination of electron–hole pairs occurring at the interface of the Cu_2O-CuO heterojunction and the formation of a depletion region (as known as space-charge region) at the interface. Therefore, the resistivity of the film has risen by an order of magnitude to 3.72×10^4 Ω-cm. Because the space-charge region has an inherent built-in potential, which is conducive to the separation of photogenerated electron-hole pairs, materials (such as nanoparticles, nanowire, thin films and so forth) with a mixed phase of Cu_2O-CuO have been extensively studied in the fields of photocatalysts, photoelectrochemical, and photovoltaic devices [3,9,23,52–54].

When the annealing time is continuously increased at 300 °C, the carrier concentration of the films increases to 8.0×10^{14} and 7.4×10^{16} cm^{-3} for 2 and 4 h, respectively. The increase in carrier concentration is related to the disappearance of the Cu_2O-CuO heterojunction in the films, at which the films have completely transformed into CuO crystal. However, the results show that, as the carrier concentration increases, the carrier mobility of the film decreases. This is because the increase in carrier concentration will increase carrier scattering and cause carrier mobility to decrease.

4. Conclusions

In this work, copper oxide films are grown on a glass substrate by the SILAR method with subsequent annealing in air. All films in this study are polycrystalline, but have three different crystal phases: as-growth and 200 °C-1 h annealed films are Cu_2O phases, the 300 °C-1 h annealed film has a Cu_2O-CuO mixed phase, and the films annealed at 300 °C for 2 and 4 h have a CuO phase. In addition, the grain size of the films increases with the increase of annealing temperature and time due to the conventional diffusion-controlled grain growth. Furthermore, as the annealing temperature and time increase, the energy bandgap of the film decreases from 1.90 to 1.34 eV, which is attributed to the crystal phase transition from Cu_2O phase to CuO phase. In addition, the resistivity, carrier concentration, and mobility of the film also vary with the annealing temperature and time. In particular, the Cu_2O-CuO mixed crystal film has a high carrier mobility of 93.7 $cm^2 \cdot V^{-1} \cdot s^{-1}$ and a low carrier concentration of 1.8×10^{12} cm^{-3}, which is attributed to the formation of Cu_2O-CuO heterojunction, and the film has potential application in photocatalyst, photoelectrochemical, and photovoltaic devices. In view of the fact that different applications usually require different material properties, this work reports the relationship between the material properties and the annealing conditions of copper oxide films. We believe that the results of this work will contribute to providing useful and valuable data for the research and applications of copper oxides.

Author Contributions: Conceptualization, W.-J.L.; Data curation, W.-J.L. and X.-J.W.; Formal analysis, W.-J.L. and X.-J.W.; Funding acquisition, W.-J.L.; Investigation, W.-J.L. and X.-J.W.; Methodology, W.-J.L.; Project administration, W.-J.L.; Resources, W.-J.L.; Supervision, W.-J.L.; Validation, W.-J.L. and X.-J.W.; Writing—original draft, W.-J.L.; Writing—review and editing, W.-J.L. All authors have read and agreed to the published version of the manuscript.

Institutional Review Board Statement: Not applicable.

Informed Consent Statement: Not applicable.

Data Availability Statement: Data sharing not applicable.

References

1.   Ogwu, A.A.; Darma, T.H.; Bouquerel, E. Electrical resistivity of copper oxide thin films prepared by reactive magnetron sputtering. *J. Achiev. Mater. Manuf. Eng.* **2007**, *24*, 172–177.

2.   Yu, J.; Hai, Y.; Jaroniec, M. Photocatalytic hydrogen production over CuO-modified titania. *J. Colloid Interface Sci.* **2011**, *357*, 223–228. [CrossRef]

3.   Dasineh Khiavi, N.; Katal, R.; Kholghi Eshkalak, S.; Masudy-Panah, S.; Ramakrishna, S.; Jiangyong, H. Visible light driven heterojunction photocatalyst of CuO-Cu$_2$O thin films for photocatalytic degradation of organic pollutants. *Nanomaterials* **2019**, *9*, 1011. [CrossRef] [PubMed]

4.   Rydosz, A. The use of copper oxide thin films in gas-sensing applications. *Coatings* **2018**, *8*, 425. [CrossRef]

5.   Steinhauer, S. Gas sensors based on copper oxide nanomaterials: A review. *Chemosensors* **2021**, *9*, 51. [CrossRef]

6.   Wang, S.B.; Hsiao, C.H.; Chang, S.J.; Lam, K.T.; Wen, K.H.; Hung, S.C.; Young, S.J.; Huang, B.R. A CuO nanowire infrared photodetector. *Sens. Actuators A* **2011**, *171*, 207–211. [CrossRef]

7.   Selman, A.M.; Mahdi, M.A.; Hassan, Z. Fabrication of Cu$_2$O nanocrystalline thin films photosensor prepared by RF sputtering technique. *Physica E* **2017**, *94*, 132–138. [CrossRef]

8.   Oku, T.; Yamada, T.; Fujimoto, K.; Akiyama, T. Microstructures and photovoltaic properties of Zn(Al)O/Cu$_2$O-based solar cells prepared by spin-coating and electrodeposition. *Coatings* **2014**, *4*, 203–213. [CrossRef]

9.   Alajlani, Y.; Placido, F.; Chu, H.O.; Bold, R.D.; Fleming, L.; Gibson, D. Characterisation of Cu$_2$O/CuO thin films produced by plasma-assisted DC sputtering for solar cell application. *Thin Solid Film.* **2017**, *642*, 45–50. [CrossRef]

10. Park, J.C.; Kim, J.; Kwon, H.; Song, H. Gram-scale synthesis of Cu$_2$O nanocubes and subsequent oxidation to CuO hollow nanostructures for lithium-ion battery anode materials. *Adv. Mater.* **2009**, *21*, 803–807. [CrossRef]

11. Hu, L.; Huang, Y.; Zhang, F.; Chen, Q. CuO/Cu$_2$O composite hollow polyhedrons fabricated from metal–organic framework templates for lithium-ion battery anodes with a long cycling life. *Nanoscale* **2013**, *5*, 4186–4190. [CrossRef] [PubMed]

12. Zhou, L.; He, Y.; Jia, C.; Pavlinek, V.; Saha, P.; Cheng, Q. Construction of hierarchical CuO/Cu$_2$O@NiCo$_2$S$_4$ nanowire arrays on copper foam for high performance supercapacitor electrodes. *Nanomaterials* **2017**, *7*, 273. [CrossRef]

13. Nathan, D.M.G.T.; Boby, S.J.M.; Basu, P.; Mahesh, R.; Harish, S.; Joseph, S.; Sagayaraj, P. One-pot hydrothermal preparation of Cu$_2$O-CuO/rGO nanocomposites with enhanced electrochemical performance for supercapacitor applications. *Appl. Surf. Sci.* **2018**, *449*, 474–484.

14. Rydosz, A.; Dyndał, K.; Andrysiewicz, W.; Grochala, D.; Marszałek, K. GLAD magnetron sputtered ultra-thin copper oxide films for gas-sensing application. *Coatings* **2020**, *10*, 378. [CrossRef]

15. Balamurugan, B.; Mehta, B.R. Optical and structural properties of nanocrystalline copper oxide thin films prepared by activated reactive evaporation. *Thin Solid Film.* **2001**, *396*, 90–96. [CrossRef]

16. Al-Kuhaili, M.F. Characterization of copper oxide thin films deposited by the thermal evaporation of cuprous oxide (Cu$_2$O). *Vacuum* **2008**, *82*, 623–629. [CrossRef]

17. Valladares, L.D.L.S.; Salinas, D.H.; Dominguez, A.B.; Najarro, D.A.; Khondaker, S.I.; Mitrelias, T.; Barnes, C.H.W.; Aguiar, J.A.; Majima, Y. Crystallization and electrical resistivity of Cu$_2$O and CuO obtained by thermal oxidation of Cu thin films on SiO$_2$/Si substrates. *Thin Solid Film.* **2012**, *520*, 6368–6374. [CrossRef]

18. Castrejón-Sánchez, V.H.; Solís, A.C.; López, R.; Encarnación-Gomez, C.; Morales, F.M.; Vargas, O.S.; Mastache-Mastache, J.E.; Sánchez, G.V. Thermal oxidation of copper over a broad temperature range-towards the formation of cupric oxide (CuO). *Mater. Res. Express* **2019**, *6*, 075909. [CrossRef]

19. Kayani, Z.N.; Umer, M.; Riaz, S.; Naseem, S. Characterization of copper oxide nanoparticles fabricated by the sol–gel method. *J. Electron. Mater.* **2015**, *44*, 3704–3709. [CrossRef]

20. Lillo-Ramiro, J.; Guerrero-Villalba, J.M.; Mota-González, M.L.; Aguirre-Tostado, F.S.; Gutiérrez-Heredia, G.; Mejía-Silva, I.; Carrillo-Castillo, A. Optical and microstructural characteristics of CuO thin films by sol gel process and introducing in non-enzymatic glucose biosensor applications. *Optik* **2021**, *229*, 166238. [CrossRef]

21. Zhu, Y.; Xu, Z.; Yan, K.; Zhao, H.; Zhang, J. One-step synthesis of CuO–Cu$_2$O heterojunction by flame spray pyrolysis for cathodic photoelectrochemical sensing of L-cysteine. *ACS Appl. Mater. Interfaces* **2017**, *9*, 40452–40460. [CrossRef] [PubMed]

22. Naveena, D.; Logu, T.; Dhanabal, R.; Sethuraman, K.; Bose, A.C. Comparative study of effective photoabsorber CuO thin films prepared via different precursors using chemical spray pyrolysis for solar cell application. *J. Mater. Sci. Mater. Electron.* **2019**, *30*, 561–572. [CrossRef]

23. Izaki, M.; Fukazawa, K.; Sato, K.; Khoo, P.L.; Kobayashi, M.; Takeuchi, A.; Uesugi, K. Defect structure and photovoltaic characteristics of internally stacked CuO/Cu$_2$O photoactive layer prepared by electrodeposition and heating. *ACS Appl. Energy Mater.* **2019**, *2*, 4833–4840. [CrossRef]

24. Rosas-Laverde, N.M.; Pruna, A.I.; Cembrero, J.; Busquets-Mataix, D. Electrodeposition of ZnO/Cu$_2$O heterojunctions on Ni-Mo-P electroless coating. *Coatings* **2020**, *10*, 935. [CrossRef]

25. Rafea, M.A.; Roushdy, N. Determination of the optical band gap for amorphous and nanocrystalline copper oxide thin films prepared by SILAR technique. *J. Phys. D Appl. Phys.* **2009**, *42*, 015413. [CrossRef]

26. Mageshwari, K.; Sathyamoorthy, R. Physical properties of nanocrystalline CuO thin films prepared by the SILAR method. *Mater. Sci. Semicond. Process* **2013**, *16*, 337–343. [CrossRef]

27. Ravichandran, A.T.; Dhanabalan, K.; Vasuhi, A.; Chandramohan, R.; Mantha, S. Morphology, bandgap, and grain size tailoring in Cu_2O thin film by SILAR method. *IEEE Trans. Nanotechnol.* **2015**, *14*, 108–112. [CrossRef]

28. Nikam, S.S.; Suryawanshi, M.P.; Bhosale, S.M.; Gaikwad, M.A.; Shinde, P.A.; Moholkar, A.V. Cu_2O thin films prepared using modified successive ionic layer adsorption and reaction method and their use in photoelectrochemical solar cells. *J. Mater. Sci. Mater. Electron.* **2016**, *27*, 1897–1900. [CrossRef]

29. Visalakshi, S.; Kannan, R.; Valanarasu, S.; Kathalingam, A.; Rajashabala, S. Effect of adsorption time on structural, optical and electronic properties of SILAR deposited CuO thin films. *J. Mater. Sci. Mater. Electron.* **2016**, *27*, 9179–9185. [CrossRef]

30. Chatterjee, S.; Saha, S.K.; Pal, A.J. Formation of all-oxide solar cells in atmospheric condition based on Cu_2O thin-films grown through SILAR technique. *Sol. Energy Mater. Sol. Cells* **2016**, *147*, 17–26. [CrossRef]

31. Nicolau, Y.F. Solution deposition of thin solid compound films by a successive ionic-layer adsorption and reaction process. *Appl. Surf. Sci.* **1985**, *22–23*, 1061–1074. [CrossRef]

32. Koch, V.M.; Barr, M.K.S.; Büttner, P.; Mínguez-Bacho, I.; Döhler, D.; Winzer, B.; Reinhardt, E.; Segets, D.; Bachmann, J. A solution-based ALD route towards $(CH_3NH_3)(PbI_3)$ perovskite *via* lead sulfide film. *J. Mater. Chem. A* **2019**, *7*, 25112–25119. [CrossRef]

33. Graniel, O.; Puigmartí-Luis, J.; Muñoz-Rojas, D. Liquid atomic layer deposition as emergent technology for the fabrication of thin films. *Dalton Trans.* **2021**, *50*, 6373–6381. [CrossRef]

34. Bayansal, F.; Kahraman, S.; Çankaya, G.; Çetinkara, H.A.; Güder, H.S.; Çakmak, H.M. Growth of homogenous CuO nano-structured thin films by a simple solution method. *J. Alloys Compd.* **2011**, *509*, 2094–2098. [CrossRef]

35. Jayakrishnan, R.; Kurian, A.S.; Nair, V.G.; Joseph, M.R. Effect of vacuum annealing on the photoconductivity of CuO thin films grown using sequential ionic layer adsorption reaction. *Mater. Chem. Phys.* **2016**, *180*, 149–155. [CrossRef]

36. Ristov, M.; Sinadinovski, G.J. Chemical deposition of Cu_2O thin films. *Thin Solid Film.* **1985**, *123*, 63–67. [CrossRef]

37. Nair, M.T.S.; Guerrero, L.; Arenas, O.L.; Nair, P.K. Chemically deposited copper oxide thin films: Structural, optical and electrical characteristics. *Appl. Surf. Sci.* **1999**, *150*, 143–151. [CrossRef]

38. Serin, N.; Serin, T.; Horzum, Ş.; Çelik, Y. Annealing effects on the properties of copper oxide thin films prepared by chemical deposition. *Semicond. Sci. Technol.* **2005**, *20*, 398–401. [CrossRef]

39. Johan, M.R.; Suan, M.S.M.; Hawari, N.L.; Ching, H.A. Annealing effects on the properties of copper oxide thin films prepared by chemical deposition. *Int. J. Electrochem. Sci.* **2011**, *6*, 6094–6104.

40. Ravichandran, A.T.; Dhanabalan, K.; Valanarasu, S.; Vasuhi, A.; Kathalingam, A. Role of immersion time on the properties of SILAR deposited CuO thin films. *J. Mater. Sci. Mater. Electron.* **2015**, *26*, 921–926. [CrossRef]

41. Cheng, H.E.; Lee, W.J. Properties of TiN films grown by atomic-layer chemical vapor deposition with a modified gaseous-pulse sequence. *Mater. Chem. Phys.* **2006**, *97*, 315–320. [CrossRef]

42. Balkanski, M.; Nusimovici, M.A.; Reydellet, J. First order Raman spectrum of Cu_2O. *Solid State Commun.* **1969**, *7*, 815–818. [CrossRef]

43. Yu, P.Y.; Shen, Y.R.; Petroff, Y.; Falicov, L.M. Resonance Raman scattering at the forbidden yellow exciton in Cu_2O. *Phys. Rev. Lett.* **1973**, *30*, 283–286. [CrossRef]

44. Dawson, P.; Hargreave, M.M.; Wilkinson, G.R. The dielectric and lattice vibrational spectrum of cuprous oxide. *J. Phys. Chem. Solids* **1973**, *34*, 2201–2208. [CrossRef]

45. Yu, P.Y.; Shen, Y.R. Resonance Raman studies in Cu_2O. I. The phonon-assisted 1*s* yellow excitonic absorption edge. *Phys. Rev. B* **1975**, *12*, 1377–1394. [CrossRef]

46. Mao, Y.; He, J.; Sun, X.; Li, W.; Lu, X.; Gan, J.; Liu, Z.; Gong, L.; Chen, J.; Liu, P.; et al. Electrochemical synthesis of hierarchical Cu_2O stars with enhanced photoelectrochemical properties. *Electrochim. Acta* **2012**, *62*, 1–7. [CrossRef]

47. Singhal, A.; Pai, M.R.; Rao, R.; Pillai, K.T.; Lieberwirth, I.; Tyagi, A.K. Copper(I) oxide nanocrystals—One step synthesis, characterization, formation mechanism, and photocatalytic properties. *Eur. J. Inorg. Chem.* **2013**, *2013*, 2640–2651. [CrossRef]

48. Wang, Z.; Pischedda, V.; Saxena, S.K.; Lazor, P. X-ray diffraction and Raman spectroscopic study of nanocrystalline CuO under pressures. *Solid State Commun.* **2002**, *121*, 275–279. [CrossRef]

49. Wang, W.; Zhou, Q.; Fei, X.; He, Y.; Zhang, P.; Zhang, G.; Peng, L.; Xie, W. Synthesis of CuO nano- and micro-structures and their Raman spectroscopic studies. *CrystEngComm* **2010**, *12*, 2232–2237. [CrossRef]

50. Nwanya, A.C.; Obi, D.; Ozoemena, K.I.; Osuji, R.U.; Awada, C.; Ruediger, A.; Maaza, M.; Rosei, F.; Ezema, F.I. Facile synthesis of nanosheet-like CuO film and its potential application as a high-performance pseudocapacitor electrode. *Electrochim. Acta* **2016**, *198*, 220–230. [CrossRef]

51. Lee, W.J.; Hon, M.H.; Chung, Y.W.; Lee, J.H. A three-dimensional nanostructure consisting of hollow TiO_2 spheres fabricated by atomic layer deposition. *Jpn. J. Appl. Phys.* **2011**, *50*, 06GH06. [CrossRef]

52. Yang, Y.; Xu, D.; Wu, Q.; Diao, P. Cu_2O/CuO bilayered composite as a high-efficiency photocathode for photoelectrochemical hydrogen evolution reaction. *Sci. Rep.* **2016**, *6*, 35158. [CrossRef] [PubMed]

53. Balik, M.; Bulut, V.; Erdogan, I.Y. Optical, structural and phase transition properties of Cu_2O, CuO and Cu_2O/CuO: Their photoelectrochemical sensor applications. *Int. J. Hydrog. Energy* **2019**, *44*, 18744–18755. [CrossRef]

54. John, S.; Roy, S.C. CuO/Cu_2O nanoflake/nanowire heterostructure photocathode with enhanced surface area for photoelectrochemical solar energy conversion. *Appl. Surf. Sci.* **2020**, *509*, 144703. [CrossRef]